Scale Transition in Steel-Concrete Interaction. I: Model

Roman Lackner[1] and Herbert A. Mang, F.ASCE[2]

Abstract: This paper deals with the analysis of reinforced concrete (RC) structures with special emphasis on modeling of the interaction between concrete and reinforcement. A new mode for consideration of the response of the composite material at the *member (structural) scale* is proposed. It is obtained from extension of the fracture energy concept, originally developed for the simulation of cracking of plain concrete, to reinforced concrete. Hereby, the fracture energy related to the opening of primary cracks is increased in order to account for bond slip between steel and concrete. This increase is determined from the distribution of bond slip by means of a one-dimensional composite model introduced at the *bar scale*. The model consists of steel bars and the surrounding concrete. Between these two components, a nonlinear bond stress–bond slip relation is considered. The obtained results at the *bar scale*, such as the average crack spacing between adjacent cracks and the load-displacement response of the composite material, form the basis for determination of the increase of the fracture energy at the *member scale*. The performance of the proposed transition of the steel-concrete interaction from the *bar scale* to the *member scale* is assessed by means of reanalysis of experiments performed on RC bars. The application of the respective material model for reinforced concrete to real-life engineering structures is reported in Part II of this series.

DOI: 10.1061/(ASCE)0733-9399(2003)129:4(393)

CE Database subject headings: Steel; Concrete; Softening; Bond stress; Stiffening.

Introduction

Research on the interaction between steel and concrete aiming at numerical analyses in structural design is characterized by a condensation of information, finally providing realistic models for a description of the composite behavior. The condensation of information is performed by a change from a lower observation scale to a higher one. In modeling of the steel-concrete interaction, three observation scales may be distinguished (Cox and Herrmann 1998) (see Fig. 1):

- The *rib scale* refers to the observation scale of single ribs of reinforcement bars. This scale is significantly smaller than the ''unit cell for concrete,'' i.e., much of the aggregate is larger than the rib.
- The action of the ribs is homogenized at the *bar scale*, allowing us to treat the reinforcement bar as well as the surrounding concrete as a continuum. The interaction between the two continua is described by means of (nonlinear) bond slip–bond stress relations. These relations are either obtained from numerical analyses performed at the *rib scale* [transition from *rib scale* to *bar scale*, see Ben Romdhane et al. (1998) and Cox and Herrmann (1998)] or from curve fitting of experimental results as provided by, e.g., Harajli et al. (1995) and Martin and Noakowski (1981).
- At the *member (structural) scale*, either a structural component or a complete structure is modeled. The reinforcement is usually described by means of the embedded-truss model in case of beam and frame analyses, or by means of the layer model in case of plate and shell analyses. In general, a uniaxial strain and stress state is assumed in the steel truss or layer. At the *member scale*, the effect of the steel-concrete interaction is commonly referred to as ''tension stiffening.'' This term stems from the capacity of the intact concrete to carry tensile forces between adjacent cracks, resulting in a higher stiffness as compared to the stiffness of the respective bare steel bars.

Over the last 20 years, several models for consideration of tension stiffening have been proposed in the open literature. Most of them belong to one of the two following categories:

- The first one is characterized by adding additional stiffness and force terms to the stiffness matrix and the force vector of the finite-element (FE) formulation. These terms may be related to the strain in the steel bar as proposed by Feenstra and De Borst (1995). Already in 1967, Ngo and Scordelis (1967) used linear springs between the reinforcing bar and the surrounding concrete in order to compute the additional stiffness and force terms. In the past, this approach was continuously improved by the introduction of nonlinear springs, as reported in Kwak and Filippou (1995) and Monti and Spacone (2000).
- The use of a specific distribution of bond stress along the reinforcement bars allows for the determination of so-called tension-stiffening factors. Already in 1982, Floegl and Mang (1982) proposed the determination of a tension-stiffening factor assuming a constant distribution of the bond stress. More recently, this approach was extended to piecewise constant distributions as reported in (Choi and Cheung 1996).

Both approaches to account for tension stiffening are characterized by a scale transition from the *bar scale* to the *member scale*.

[1]Research Assistant, Institute for Strength of Materials, Vienna Univ. of Technology, Karlsplatz 13/202, A-1040 Vienna, Austria. E-mail: Roman.Lackner@tuwien.ac.at

[2]Professor, Institute for Strength of Materials, Vienna Univ. of Technology, Karlsplatz 13/202, A-1040 Vienna, Austria. E-mail: Herbert.Mang@tuwien.ac.at

Note. Associate Editor: Franz-Josef Ulm. Discussion open until September 1, 2003. Separate discussions must be submitted for individual papers. To extend the closing date by one month, a written request must be filed with the ASCE Managing Editor. The manuscript for this paper was submitted for review and possible publication on December 17, 2001; approved on July 24, 2002. This paper is part of the ***Journal of Engineering Mechanics***, Vol. 129, No. 4, April 1, 2003. ©ASCE, ISSN 0733-9399/2003/4-393–402/$18.00.

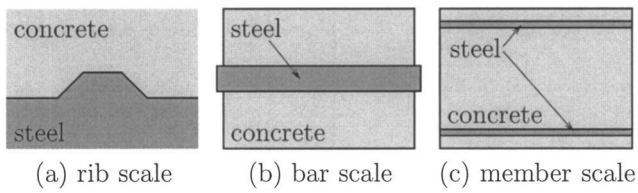

Fig. 1. Scales of observation in modeling of steel–concrete interaction according to Cox and Herrmann (1998)

However, different methods were used. The introduction of nonlinear springs is based on micromechanical considerations. For determination of tension-stiffening factors, as reported in Floegl and Mang (1982) and Choi and Cheung (1996), the principle of virtual work was used.

In order to circumvent the shortcomings of the two approaches such as the lack of robustness when considering nonlinear springs in the FE model or constant distributions of the bond slip as used by Floegl and Mang (1982) and Choi and Cheung (1996), a new mode of scale transition is presented in this paper. It is based on the fracture energy concept (Hillerborg et al. 1976). This concept has been successfully employed over the last decades for the analysis of plain concrete by means of the FEM [see, e.g., Feenstra (1993); Etse and Willam (1994); Meschke et al. (1998); Pivonka et al. (2001)]. The proposed transition for the consideration of tension stiffening at the *member scale* is based on the extension of this concept towards reinforced concrete. The paper is divided into two parts:

The first part deals with the aforementioned extension of the fracture energy concept. Starting point is the determination of the average crack spacing of the stabilized crack pattern of reinforced concrete. For this purpose, a one-dimensional composite model will be introduced at the *bar scale*. This model will be employed for the determination of the maximum crack spacing. The average crack spacing, which will be related to the maximum crack spacing, defines the length of the one-dimensional composite model when employed for the determination of the influence of tension stiffening on the load-carrying behavior of reinforced concrete. Hereby, cracks are assumed to open simultaneously at a distance of the average crack spacing. Thereafter, the results obtained at the *bar scale* will be transferred to the *member scale*. The proposed mode of scale transition will be assessed by means of reanalyses of uniaxial experiments conducted by Rostásy et al. (1976).

The second part of the paper is devoted to the application of the proposed material model for reinforced concrete to real-life engineering structures.

Fracture Energy Concept for Plain Concrete (Hillerborg et al. 1976)

Depending on the type of loading, the microstructure of concrete leads to different deformation characteristics and failure modes. Under tensile loading, the relatively low adhesive strength of the cement-aggregate interface causes a brittle material behavior, characterized by the development of cracks. Within the fracture energy concept, the discrete jumps in the displacement field at these cracks $[\![\mathbf{u}]\!]$ are replaced by the respective distribution of plastic strains (smeared crack approach)

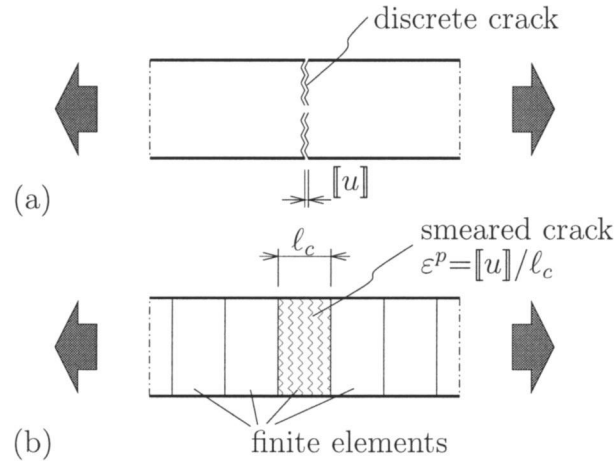

Fig. 2. One-dimensional illustration of smeared crack approach applied to plain concrete: (a) discrete crack width $[\![u]\!]$ and (b) its representation by means of respective distribution of plastic strain ε^p (ℓ_c: size of finite element)

$$[\![\mathbf{u}]\!] \rightarrow \int_{\ell_c} \boldsymbol{\varepsilon}^p dx_n \tag{1}$$

where x_n = local coordinate normal to the crack. For plain concrete, the zone representing the crack by means of plastic strains is localized in one finite element (see Fig. 2). Hence, the width of the plastic zone ℓ_c is related to the element size [see, e.g., Oliver (1989) and Huemer et al. (1999)].

Because of cracking, the tensile strength $\overline{q}$ is decreasing. This decrease is considered by means of an exponential softening law, given by

$$\overline{q} = f_{tu} \exp(-\alpha/\overline{\alpha}) \tag{2}$$

where f_{tu} = tensile strength at the onset of cracking and α = internal variable of the employed failure criterion. According to the fracture energy concept, the calibration parameter $\overline{\alpha}$ is obtained from setting the area under the employed softening relation Eq. (2) equal to the fracture energy of one crack divided by the respective crack width, i.e., equal to G^f/ℓ_c

$$\frac{G^f}{\ell_c} = \int_0^\infty \overline{q} d\alpha = \int_0^\infty f_{tu} \exp(-\alpha/\overline{\alpha}) d\alpha = f_{tu}\overline{\alpha}. \tag{3}$$

Reformulation of Eq. (3) yields the calibration parameter $\overline{\alpha}$ as a function of the element size ℓ_c and the fracture energy G^f

$$\overline{\alpha} = \frac{G^f}{\ell_c f_{tu}} \tag{4}$$

Fracture Energy Concept for Reinforced Concrete

The presence of steel bars in reinforced concrete results in a distribution of cracks, finally giving a stabilized crack pattern. The average distance between two primary cracks ℓ_s depends on the geometric properties (concrete cover, bar diameter, etc.) and the material properties (Young's moduli of concrete and steel, tensile strength of concrete, etc.). In contrast to assuming localization of plastic strains in a single finite element as in the case of FE analyses of plain concrete, the presence of the reinforcement allows for an increase of the applied load even if cracking of concrete was initiated. As long as no relative displacement between

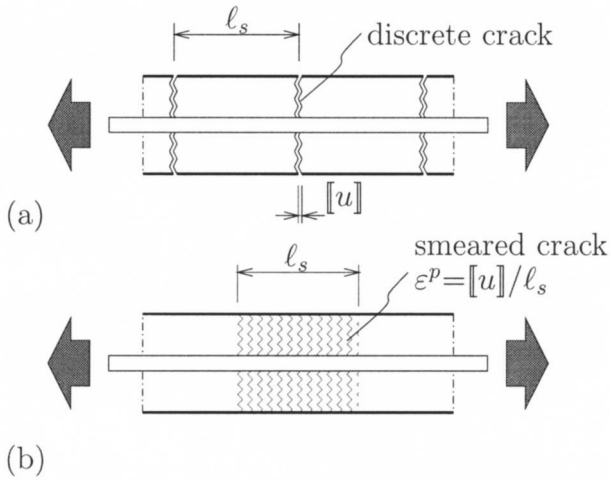

Fig. 3. One-dimensional illustration of smeared crack approach applied to reinforced concrete: (a) discrete crack width $[\![u]\!]$ and (b) its representation by means of respective distribution of plastic strain ε^p (ℓ_s: spacing of primary cracks)

steel and concrete is considered, the increasing load causes cracking in every element intersected by the steel bar. Hence, each primary crack is distributed over the respective crack spacing ℓ_s along the steel bar and is represented by the respective plastic strains (see Fig. 3). In the context of the fracture energy concept, the width of the plastic zone is equal to the average crack spacing ℓ_s. Hence, consideration of a stabilized crack pattern in the calibration of the fracture criterion is obtained by replacing ℓ_c in Eq. (4) by the average crack spacing ℓ_s, giving

$$\bar{\alpha} = \frac{G^f}{\ell_s f_{tu}} \tag{5}$$

Determination of Average Crack Spacing ℓ_s

The average crack spacing ℓ_s of the stabilized crack pattern is computed in two steps:

1. In the first step, the maximum crack spacing between two primary cracks, $\ell_{s,\max}$, is evaluated. The maximum crack spacing is defined as the distance between two adjacent cracks opening simultaneously, with the concrete stress at midpoint between these adjacent cracks being equal to the tensile strength.
2. In the second step, the average crack spacing ℓ_s is estimated from $\ell_{s,\max}$ following CEB-FIP (1990). According to CEB-FIP (1990), ℓ_s can be set equal to $(2/3)\ell_{s,\max}$.

In the following, the determination of $\ell_{s,\max}$ is outlined. It is based on a one-dimensional composite model introduced at the *bar scale* of the steel-concrete interaction.

One-dimensional Composite Model

For the evaluation of $\ell_{s,\max}$, a one-dimensional model of length ℓ is used (see Fig. 4). The model consists of the reinforcement given by the steel area per unit length, a_s (mm^2/m), and the surrounding concrete. The concrete area is given by the effective tension height of concrete, $h_{c,\text{eff}}$ (m). It is estimated according to

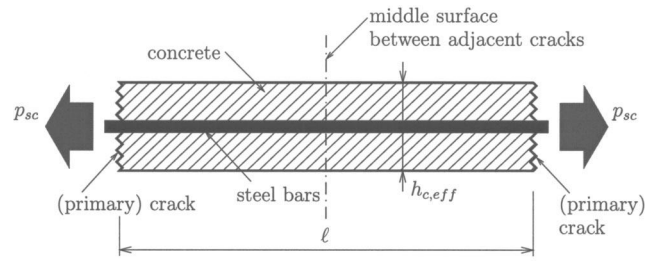

Fig. 4. One-dimensional composite model at *bar scale* ($h_{c,\text{eff}}$: effective tension height of concrete; p_{sc}: force acting on composite structure)

CEB-FIP (1990) recommendations. For the case of distributed reinforcement by means of, e.g., reinforcement grids, $h_{c,\text{eff}}$ is obtained as depicted in Fig. 5.

The length of the model ℓ is equal to the distance between two primary cracks. Between these cracks both steel and concrete are treated as a continuum. A nonlinear bond stress–bond slip relation is considered (bond slip is the relative displacement between steel and concrete). In the following, the distribution of the bond slip will be determined for this relation.

Determination of Bond Slip Distribution

The change of bond slip s between the steel bars and the surrounding concrete is equal to the difference between the steel and concrete strains, ε_s and ε_c,

$$\frac{ds}{dx} = \varepsilon_s - \varepsilon_c = \frac{\sigma_s}{E_s} - \frac{\sigma_c}{E_c} \tag{6}$$

where σ_s=stress in the steel and σ_c=stress in the surrounding concrete. E_s and E_c=Young's moduli for steel and concrete, respectively. The load p_{sc}, acting on the composite structure (see Fig. 4), must be carried by the reinforcement and the surrounding concrete. This results in

$$p_{sc} = \sigma_s a_s + \sigma_c h_{c,\text{eff}} \rightarrow \sigma_c = \frac{p_{sc}}{h_{c,\text{eff}}} - \sigma_s \frac{a_s}{h_{c,\text{eff}}} \tag{7}$$

Inserting Eq. (7) in Eq. (6) and differentiating with respect to x yields

$$\frac{d^2 s}{dx^2} = \frac{d\sigma_s}{dx}\frac{1+n\rho_s}{E_s} \quad \text{with} \quad n = \frac{E_s}{E_c}, \quad \rho_s = \frac{a_s}{h_{c,\text{eff}}} \tag{8}$$

noting that p_{sc} must be constant in order to satisfy the equilibrium condition in direction of the steel bars. Hence, $dp_{sc}/dx = 0$.

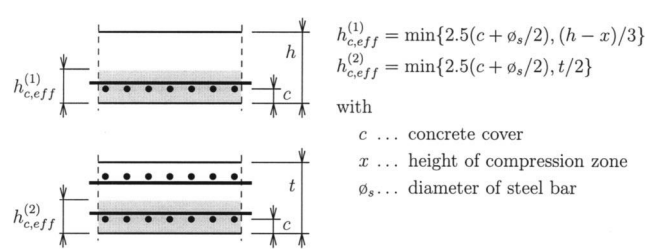

Fig. 5. On evaluation of effective tension height of concrete $h_{c,\text{eff}}$ for different arrangements of reinforcement according to CEB-FIP (1990)

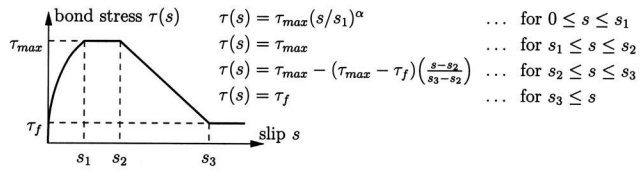

Fig. 6. Bond stress–bond slip relation according to CEB-FIP (1990)

$d\sigma_s/dx$ is obtained as the force transferred from the steel bars to the concrete (bond force) divided by the cross-sectional area of the steel bars

$$\frac{d\sigma_s}{dx} = \frac{n_s \varnothing_s \pi}{a_s}\tau(s) = \frac{4}{\varnothing_s}\tau(s) \tag{9}$$

where n_s = number of steel bars per unit length and $\varnothing_s$ = diameter of the reinforcement. $\tau(s)$ is the bond stress which is a function of s. Substituting Eq. (9) into Eq. (8) yields the differential equation for the bond slip as (Rehm 1961)

$$\frac{d^2s}{dx^2} - k\tau(s) = 0 \quad \text{with} \quad k = \frac{4}{\varnothing_s}\frac{1+n\rho_s}{E_s} = \text{constant} > 0 \tag{10}$$

In this paper, the bond stress–bond slip relation given in CEB-FIP (1990) is used (see Fig. 6). This relation is in accordance with experimental data such as reported in Ciampi et al. (1981), Eligehausen et al. (1983), and Ciampi et al. (1982). In order to avoid numerical problems arising from spatial discretization at the *bar scale*, an analytical solution for the bond slip s is derived. The origin of the coordinate system with the axis x coincides with the onset of the bond slip; the value of $s(x)$ increases with increasing x. According to the nonsmooth bond stress–bond slip relation depicted in Fig. 6, the analytical solution consists of four parts. The first part is related to the nonlinear part of the bond stress–bond slip diagram. It contains the onset of bond slip at $x=0$, characterized by $s=0$. Moreover, a perfect bond at the onset of bond slip gives $\varepsilon_c = \varepsilon_s$, yielding $ds/dx = 0$ at $x=0$ [see Eq. (6)]. For this type of boundary conditions, the analytical solution of the differential Eq. (10) referring to the first (nonlinear) part of the bond stress–bond slip diagram is given in the Appendix. For the remaining parts, characterized by linear and constant bond stress–bond slip relations, respectively, the constant coefficients of the solutions given in the Appendix must be adjusted to the transition conditions, i.e., to the values of s and ds/dx at the end of the preceding part of the analytical solution of $s(x)$. Fig. 7 shows the bond slip distribution obtained for a specific set of parameters k, s_1, s_2, s_3, τ_f, and τ_{max}. For this set, characterized by $s_1 = s_2$, the analytical solution consists of three parts.

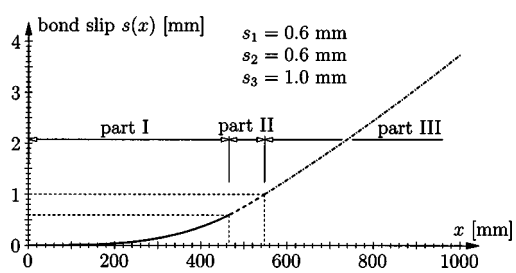

Fig. 7. Analytical solution for bond slip consisting of three parts, with $k = 2.6 \times 10^{-6}$ mm/N, $\tau_{max} = 8.25$ N/mm^2, and $\tau_f = 0.15\tau_{max}$

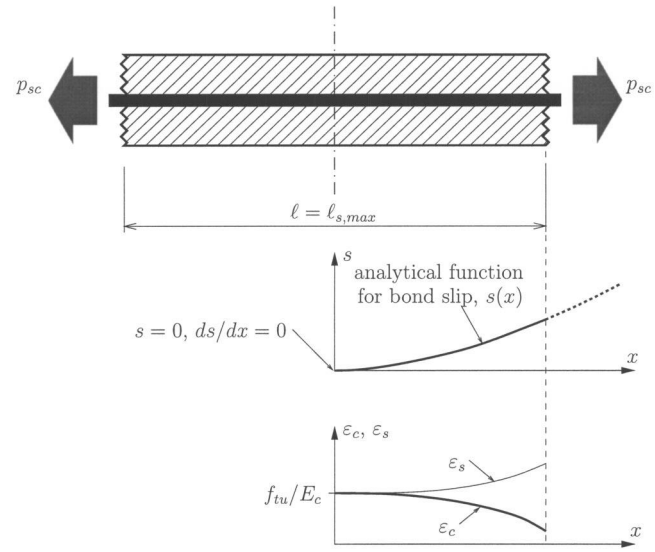

Fig. 8. One-dimensional composite model at *bar scale:* distribution of bond slip and strain in steel and concrete for case of $\ell = \ell_{s,\max}$

Determination of Maximum Crack Spacing $\ell_{s,\max}$

The maximum spacing between two adjacent primary cracks $\ell_{s,\max}$ is computed at the *bar scale* employing the one-dimensional composite model depicted in Fig. 6. The length of the model ℓ which, for the present case, is equal to the maximum crack spacing, must be determined. For this purpose, the analytical solution for the bond slip $s(x)$ is employed. The onset of the bond slip characterized by $x=0$ is located at the middle surface between adjacent cracks (see Fig. 8). Consequently, the maximum stress in the concrete is obtained at $x=0$. According to the definition of the maximum crack spacing, it is equal to the tensile strength of concrete, f_{tu}.

The maximum crack spacing is computed in an iterative manner. The starting point is the known force in the concrete at the middle surface between the two adjacent cracks, i.e., at $x=0$. It is given by

$$p_c(0) = \sigma_c h_{c,\text{eff}} = f_{tu} h_{c,\text{eff}} \tag{11}$$

Then, the force in the concrete at the crack face, i.e., at $x = \ell/2$, is computed using the analytical solution for the bond slip $s(x)$

- First, $p_c(\ell/2)$ is obtained from consideration of the stress transfer from concrete to steel via bond stress $\tau[s(x)]$, reading

$$p_c(\ell/2) = p_c(0) - n_s \int_0^{\ell/2} \varnothing_s \pi \tau[s(x)]dx \tag{12}$$

  where n_s = number of steel bars per unit length.
- The second mode of determination of $p_c(\ell/2)$ is based on the crack opening $[\![u]\!]$ at $x = \ell/2$, given by $[\![u]\!] = 2s(\ell/2)$. The factor 2 accounts for the fact that bond slip takes place on both sides of the opening primary crack. Assuming exponential softening, the force in the concrete is obtained as

$$p_c(\ell/2) = f_{tu} h_{c,\text{eff}} \exp(-[\![u]\!]/[\![\overline{u}]\!]) \tag{13}$$

  where $[\![\overline{u}]\!]$ = calibration parameter for the exponential softening law, with $[\![\overline{u}]\!] = G^f/f_{tu}$. Note that no length scale is required for the calibration of the softening law (13). In contrast to Eq. (2), the softening law (13) is controlled by the crack width $[\![u]\!]$ itself.

During the iteration, the length of the composite model ℓ is continuously increased until both modes of determination of $p_c(\ell/2)$

give the same result. If this is the case, ℓ represents the maximum crack spacing, giving $\ell_{s,\max}=\ell$. Finally, the average crack spacing can be estimated according to CEB-FIP (1990) as $\ell_s=(2/3)\ell_{s,\max}$.

Tension Stiffening

The opening of cracks is characterized by a decrease of the stress in the concrete which finally becomes zero. However, the intact concrete between the primary cracks still carries tensile stresses. The stress transfer from steel at the location of primary cracks to the intact concrete is mainly controlled by bond slip. Because of the residual load-carrying capacity of cracked concrete in consequence of bond slip, the response of cracked reinforced concrete specimens is stiffer than the one of an otherwise identical steel bar which is not embedded in cracked concrete. This effect is referred to as tension stiffening.

So far, the average crack spacing of reinforced concrete ℓ_s was computed. It allows for consideration of the opening of primary cracks within the fracture energy concept. So far, however, the effect of tension stiffening was disregarded. In order to consider this effect in the context of the fracture energy concept, the response of the composite material is computed at the *bar scale*. Again, the one-dimensional model is employed. The length of the model ℓ is set equal to the average crack spacing ℓ_s. The response of the composite bar is divided in the following three stages:

1. In the first stage, the concrete stress is smaller than the tensile strength, i.e., $\sigma_c<f_{tu}$. No crack has opened so far. Hence, bond slip is not considered. This stage is terminated by the initiation of cracking of concrete, with $\sigma_c=f_{tu}$. At this loading state, the stress in the reinforcement is obtained from the compatibility of strains between steel and concrete as

$$\sigma_s=E_s\varepsilon_s=E_s\varepsilon_c=E_s\frac{f_{tu}}{E_c}=nf_{tu} \tag{14}$$

The force acting on the composite bar is given by

$$p_{sc}=p_c+p_s=h_{c,\text{eff}}\,\sigma_c+a_s\sigma_s=h_{c,\text{eff}}\,f_{tu}(1+n\rho_s) \tag{15}$$

The respective displacement measured at the crack face is obtained from

$$u(\ell/2)=\varepsilon_c\frac{\ell}{2}=\frac{f_{tu}}{E_c}\frac{\ell}{2} \tag{16}$$

2. The second stage is characterized by the simultaneous opening of the two adjacent primary cracks. The onset point of bond slip $x=0$ is located between the crack face and the middle surface between the primary cracks (see Fig. 9). The force transferred via bond slip is obtained as

$$p_{bs}(\overline{x})=n_s\int_0^{\overline{x}}\varnothing_s\pi\tau[s(x)]dx \tag{17}$$

where $x=\overline{x}=$location of the crack face. The force in the concrete at the crack face is obtained from the bond slip at $x=\overline{x}$, $s(\overline{x})$,

$$p_c(\overline{x})=h_{c,\text{eff}}\,f_{tu}\exp(-[\![u]\!]/[\![\overline{u}]\!]) \tag{18}$$

with $[\![u]\!]=2s(\overline{x})$. p_c at the onset of bond slip, i.e., at $x=0$, is given by $p_c(0)=p_c(\overline{x})+p_{bs}$. At this point, $\varepsilon_s=\varepsilon_c$. Hence, the respective force in the reinforcement can be computed

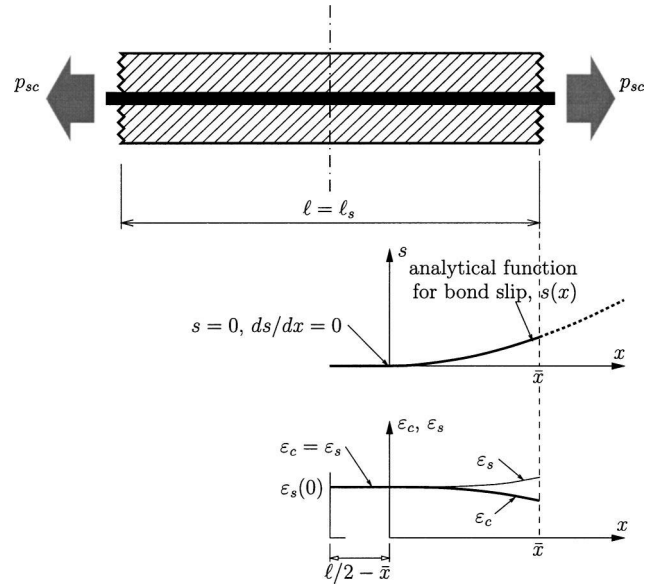

Fig. 9. One-dimensional composite model at *bar scale:* distribution of bond slip and strain in steel and concrete, respectively, for onset of bond slip located between crack face and middle surface between adjacent cracks

from

$$p_s(0)=a_s\sigma_s=a_sE_s\varepsilon_s=a_sE_s\varepsilon_c=a_s\frac{E_s}{E_c}\sigma_c=a_s\frac{E_s}{E_c}\frac{p_c(0)}{h_{c,\text{eff}}}=\rho_s np_c(0) \tag{19}$$

where use of the definition for n and ρ_s [see Eq. (8)] was made. The force acting on the composite bar at the onset of slip is given by

$$p_{sc}(0)=p_c(0)+p_s(0)=(1+\rho_s n)p_c(0) \tag{20}$$

Recall, p_{sc} must be constant in order to satisfy the equilibrium condition in direction of the steel bar. Hence, $p_{sc}(x)=p_{sc}(0)=$constant. The displacement u at the crack face is computed from integration of the strains in the steel bar (see Fig. 9), reading

$$u(\overline{x})=\varepsilon_s(0)\left(\frac{\ell}{2}-\overline{x}\right)+\int_0^{\overline{x}}\left(\varepsilon_s(0)+\frac{p_{bs}(x)}{a_sE_s}\right)dx \tag{21}$$

with

$$p_{bs}(x)=n_s\int_0^x\varnothing_s\pi\tau[s(x)]dx. \tag{22}$$

$p_{sc}(\overline{x})=p_{sc}(0)$ and the corresponding displacement $u(\overline{x})$ are determined for different values of $\overline{x}$, with $0\leqslant\overline{x}\leqslant\ell/2$.

3. In the third stage of the response of the composite bar, the onset of bond slip has reached the middle surface. Hence, $\overline{x}=\ell/2$. From this loading state on, a constant load transfer from steel to concrete is assumed, with

$$p_{bs}=n_s\int_0^{\ell/2}\varnothing_s\pi\tau[s(x)]dx. \tag{23}$$

Bond slip at the crack face $s(\ell/2)$ is continuously increasing during this part of the simulation. The force in the concrete at the crack face is obtained from the exponential softening law, reading

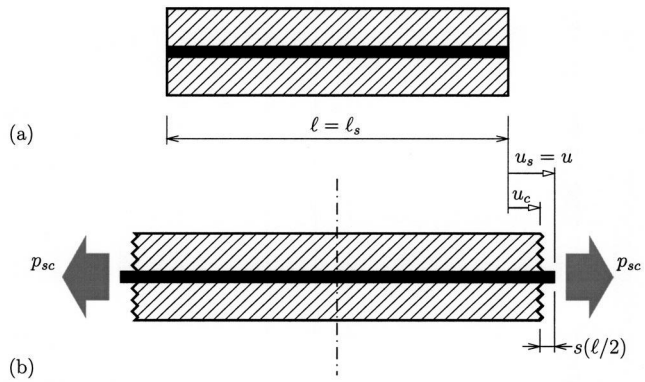

Fig. 10. One-dimensional composite model at *bar scale:* (a) undeformed and (b) deformed configuration

$$p_c(\ell/2) = f_{tu} h_{c,\text{eff}} \exp(-[\![u]\!]/[\![\overline{u}]\!]), \quad \text{with } [\![u]\!] = 2s(\ell/2) \tag{24}$$

The force in the concrete at the middle surface is obtained from $p_c(0) = p_c(\ell/2) + p_{bs}$. The force in the reinforcement is computed from the compatibility condition of the displacement at the crack face (see Fig. 10)

$$u_s - u_c = s(\ell/2) \tag{25}$$

Replacing the displacements in Eq. (25) by the respective integrals over the strains gives

$$\int_0^{\ell/2} \left[\varepsilon_s(0) + \frac{p_{bs}(x)}{a_s E_s} \right] dx - \int_0^{\ell/2} \left[\varepsilon_c(0) - \frac{p_{bs}(x)}{h_{c,\text{eff}} E_c} \right] dx = s(\ell/2) \tag{26}$$

Using $\varepsilon_s(0) = p_s(0)/(a_s E_s)$ and $\varepsilon_c(0) = p_c(0)/(h_{c,\text{eff}} E_c)$ gives the force in the reinforcement at the middle surface as

$$p_s(0) = \frac{a_s E_s}{\ell/2} \left\{ s(\ell/2) + \int_0^{\ell/2} \left[\frac{p_c(0) - p_{bs}(x)}{h_{c,\text{eff}} E_c} - \frac{p_{bs}(x)}{a_s E_s} \right] dx \right\} \tag{27}$$

Finally, the force in the composite bar is obtained as $p_{sc}(x) = p_{sc}(0) = p_c(0) + p_s(0)$. The corresponding displacement u is equal to the displacement of the steel bar at $x = \ell/2$ (see Fig. 10). It is computed from the first integral in Eq. (26), reading

$$u = \int_0^{\ell/2} \left[\frac{p_s(0) + p_{bs}(x)}{a_s E_s} \right] dx \tag{28}$$

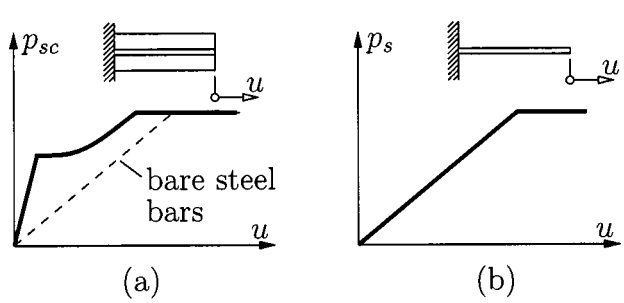

Fig. 11. Schematic load-displacement relation at the *bar scale* for (a) embedded steel bars and (b) bare steel bars

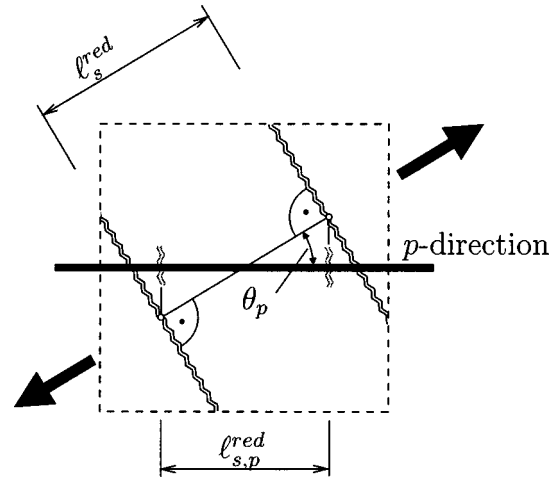

Fig. 12. Definition of reduced average crack spacing ℓ_s^{red} for reinforcement bars intersecting cracks nonorthogonally (CEB-FIP 1990)

The analysis is terminated when the yielding of steel is encountered at the location of the crack. Finally, a load-displacement response of the composite bar as depicted in Fig. 11(a) is obtained.

Transition from Bar Scale to Member Scale

The input parameter for the fracture energy concept for the simulation of cracking of plain concrete is the energy released during the opening of one single crack, referred to as fracture energy. The fracture energy is assumed to be a constant material property. In the extension of the fracture energy concept to reinforced concrete, the released energy in consequence of both cracking of concrete *and* bond slip serves as the input parameter. Consequently, the main objective during the transition of the steel-concrete interaction from the *bar scale* to the *member scale* is the preservation of the released energy. Based on the already computed load-displacement response of the composite material, $p_{sc} - u$ response [see Fig. 11(a)], and the reaction force for the respective bare steel bars p_s [see Fig. 11(b)], the energy release in consequence of cracking of concrete and bond slip at the *bar scale*-related to the area of concrete-is obtained as

$$\mathcal{W} = \mathcal{W}_{sc} - \mathcal{W}_s = \int_0^{\infty} \frac{p_{sc} - p_s}{h_{c,\text{eff}}} du \tag{29}$$

At the *member (structural) scale*, $\mathcal{W}$ is assigned to the material response of concrete. p_{sc} and p_s [see Eq. (29)] were computed on the basis of a composite model of length ℓ_s. Hence, the extension of the calibration of the fracture criterion given in Eq. (5) to consideration of tension stiffening takes the form

$$\overline{\alpha} = \frac{\mathcal{W}}{\ell_s f_{tu}}. \tag{30}$$

Eq. (30) can be rewritten in the form

$$\overline{\alpha} = \frac{G^f}{\ell_s^{\text{red}} f_{tu}} \tag{31}$$

where ℓ_s^{red}=*artificially reduced* average crack spacing, defined as $\ell_s^{\text{red}} = \ell_s G^f / \mathcal{W}$. The two modes of computing $\overline{\alpha}$ according to Eqs. (30) and (31) are equal for the one-dimensional case. For the plane-stress situation, however, use of the reduced average crack spacing ℓ_s^{red} is advantageous for the extension of the calibration to

Table 1. Geometric Data and Material Properties Provided for Specimens V1 to V4 According to Rostásy et al. (1976) (f_{sy}: yield stress of steel)

Experiment	$\varnothing_s$ (mm)	A_s (mm^2)	E_s (N/mm^2)	f_{sy} (N/mm^2)	A_c (mm^2)	$f_{cu,\text{cube}}$ (N/mm^2)	f_{tu} (N/mm^2)	ρ_s (%)
V1	6	565	209,000	611	150,000	7.5	0.98	0.375
V2	8	503	206,000	544	150,000	8.7	0.85	0.333
V3	8	1,005	206,000	544	150,000	10.0	1.24	0.667
V4	8	1,508	206,000	544	150,000	8.8	0.98	1.000

reinforcement bars intersecting the crack nonorthogonally and to orthogonally reinforced concrete members.

Extension to Aligned Cracks

For the general case of reinforcement bars intersecting cracks nonorthogonally, ℓ_s^{red} is computed from (CEB-FIP 1990)

$$\ell_s^{\text{red}} = \frac{\ell_{s,p}^{\text{red}}}{|\cos\theta_p|} \tag{32}$$

where θ_p = angle between the direction of the reinforcement (p) and the normal to the cracks (see Fig. 12). In Eq. (32), $\ell_{s,p}^{\text{red}}$ refers to the reduced average crack spacing corresponding to cracks normal to the reinforcement.

Extension to Orthogonally Reinforced Concrete Members

For orthogonally reinforced concrete members, the described calculation procedure for the evaluation of the reduced average crack spacing is performed for both directions of reinforcement, yielding $\ell_{s,p}^{\text{red}}$ and $\ell_{s,q}^{\text{red}}$ (p and q denoting the two orthogonal directions). ℓ_s^{red} for aligned cracks is then given by (CEB-FIP 1990)

$$\ell_s^{\text{red}} = \left[\frac{|\cos\theta_p|}{\ell_{s,p}^{\text{red}}} + \frac{|\sin\theta_p|}{\ell_{s,q}^{\text{red}}}\right]^{-1}. \tag{33}$$

Verification of Model

The proposed transition of the steel-concrete interaction from the *bar scale* to the *member (structural) scale* is assessed by the recalculation of RC bars with variable reinforcement ratios ρ_s and bar diameters $\varnothing_s$. The bars are subjected to uniaxial tension.

Material Properties

Table 1 contains the geometric data and the provided material properties for the considered specimens V1 to V4 (Rostásy et al. 1976). The missing material parameters, such as Young's modulus and the fracture energy of concrete, are computed from the compressive strength following the CEB-FIP recommendations (CEB-FIP 1990)

Table 2. Missing Material Parameters Computed According to CEB-FIP Recommendations (CEB-FIP 1990)

Experiment	f_{cu} (N/mm^2)	E_c (N/mm^2)	G^f (Nmm/mm^2)
V1	6.0	18,133	0.0210
V2	7.0	19,090	0.0234
V3	8.0	19,959	0.0257
V4	7.0	19,090	0.0234

$$f_{cu} = 0.8 f_{cu,\text{cube}}, \quad E_c = E_{c0}\left(\frac{f_{cu}}{f_{cu0}}\right)^{1/3}, \quad G^f = G_0^f\left(\frac{f_{cu}}{f_{cu0}}\right)^{0.7} \tag{34}$$

where $f_{cu0} = 10$ N/mm^2 and $E_{c0} = 21{,}500$ N/mm^2. G_0^f depends on the maximum aggregate size $d_{\max}$. In the present case of $d_{\max} = 16$ mm it is given by $G_0^f = 0.03$ Nmm/mm^2. Table 2 contains the computed material parameters.

Use of the experimentally obtained values for the tensile strength for concrete (see Table 1) led to deviations between the experimental and numerical results at the onset of cracking of the reinforced bars. Taking into account the large scatter of these values, they were adapted to the experimentally obtained load-displacement curves of the RC bars. The adaptation was performed such that good agreement of the load at the onset of cracking between the experiments and the numerical results was obtained. The employed tensile strengths and the computed data needed for calibration of the fracture criterion for concrete are listed in Table 3. It contains the average spacing of primary cracks ℓ_s and the reduced average crack spacing ℓ_s^{red}. It is noteworthy that the reduced average crack spacing is 15 to 20 times smaller than the average crack spacing ℓ_s, i.e., $\ell_s/\ell_s^{\text{red}} = \mathcal{W}/G^f = 15$–$20$. The rather high value of the ratio $\ell_s/\ell_s^{\text{red}}$ is a consequence of the poor concrete employed in the experimental tests by (Rostásy et al. 1976), characterized by $G^f < 0.026$ Nmm/mm^2. For the concrete/shotcrete dealt with in Part II of this series (Lackner and Mang 2003), $\ell_s/\ell_s^{\text{red}}$ is mainly between 5 and 10. This agrees with numerical results given in Feenstra (1993) [see, e.g., reanalysis of panels tested by Kollegger (1988)].

Crack/Yield Criteria for Concrete and Steel

The crack/yield criteria employed for simulation of cracking of concrete and yielding of steel are given as

$$f = \sigma - \overline{q} \leq 0, \tag{35}$$

where σ denotes the uniaxial stress and $\overline{q}$ represents the respective material strength. For concrete, the exponential softening law according to Eq. (2) is used, with $\overline{\alpha}$ computed according to Eq. (31). For the reinforcement, a nonlinear hardening/softening relation is considered (see Fig. 13).

Table 3. Adapted Tensile Strengths and Computed Parameters for Calibration of Fracture Criterion for Concrete, ℓ_s and ℓ_s^{red}

Experiment	f_{tu} (N/mm^2)	ℓ_s (mm)	ℓ_s^{red} (mm)
V1	1.10	481	24
V2	0.90	541	32
V3	1.15	419	27
V4	1.25	380	23

Note: For bond stress–bond slip relation, the following parameters were used: $s_1 = 0.6$ mm; $s_2 = 0.6$ mm; $s_3 = 1.0$ mm; $\tau_{\max} = 2\sqrt{f_{cu}}$; $\tau_f = 0.15\tau_{\max}$; and $\alpha = 0.4$ (CEB-FIP 1990).

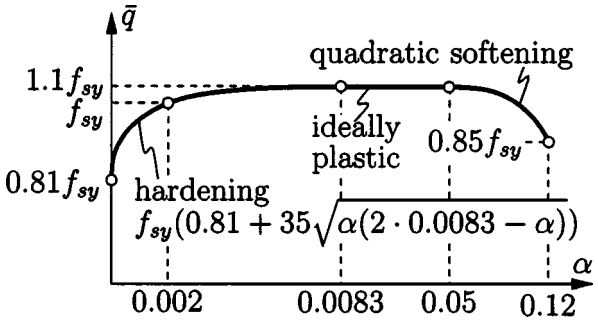

Fig. 13. Employed hardening/softening relation for cold-drawn steel bars (Dilger 1966) (f_{sy}: yield stress)

For both concrete and steel, the internal variable α is set equal to the respective plastic strain.

Numerical Results

Fig. 14(a) contains the numerical results from the simulation of the RC Bars V1 to V4. They indicate good agreement with the experimental results. Fig. 14(b) shows the influence of the proposed mode of consideration of tension stiffening by means of the reduced average crack spacing for the RC Bar V3. For this purpose, a dimensionless parameter β is introduced. $\beta=1$ represents full consideration of tension stiffening, whereas in case of $\beta=0$ tension stiffening is neglected. A continuous decrease of the influence of tension stiffening in the material model for concrete is achieved by increasing the reduced average crack spacing ℓ_s^{red} from its original value, i.e., $\ell_s^{\mathrm{red}}=27$ mm, to the average crack spacing $\ell_s=419$ mm

$$\ell_s^{\mathrm{red}}(\beta)=419(1-\beta)+27\beta[\mathrm{mm}] \tag{36}$$

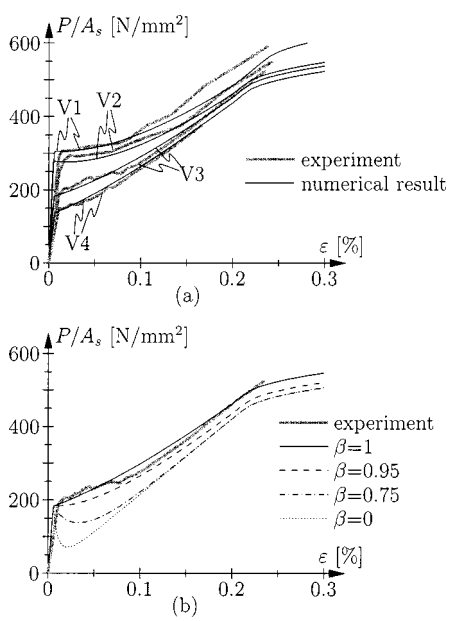

Fig. 14. $P/A_s-\varepsilon$ curves on basis of proposed mode of transition of steel-concrete interaction to *member scale:* numerical results for (a) Experiments V1 to V4 and (b) reduction of influence of tension stiffening for Experiment V3 by means of dimensionless parameter β. A_s denotes area of reinforcement bars of respective RC bar

Fig. 14(b) contains numerical results obtained for $\beta \in\{1,0.95,0.75,0\}$. A decreasing value of β results in an increase of the reduced average crack spacing ℓ_s^{red} [see Eq. (36)]. As ℓ_s^{red} increases, less cracks are assumed to open and, hence, less energy is released. Consequently, the load-carrying capacity of the RC Bar V3 is underestimated.

Conclusions

In this paper, the transition of the material response resulting from the steel-concrete interaction in reinforced concrete (RC) from the *bar scale* to the *member (structural) scale* was dealt with. For this purpose, the fracture energy concept, commonly employed for the analysis of plain concrete, was extended towards consideration of the reinforcement.

At the *bar scale*, a one-dimensional composite model was introduced. It consists of steel bars and the part of concrete assigned to the respective reinforcement. The interaction between steel and concrete was modeled by means of a nonlinear bond stress–bond slip relation. The response of the composite model was transferred to the *member scale* by increasing the energy related to cracking of concrete.

The performance of the proposed consideration of the steel-concrete interaction at the *member scale* was assessed by means of reanalyses of experiments reported in (Rostásy et al. 1976). Based on the obtained results, the following conclusions can be drawn:

- Good agreement between the numerical result and the available experimental data was observed.
- Disregard of the steel-concrete interaction in the calibration of the concrete model resulted in an underestimation of the load-carrying behavior of the investigated RC bars.

In contrast to previous approaches for the transition of the steel-concrete interaction from the *bar scale* to the *member (structural) scale*, the proposed mode allows consideration of a nonlinear bond stress–bond slip relation. The computations at the *bar scale* for determination of calibration parameters required at the *member scale* were performed in advance. Hence, no additional analyses are needed during structural analysis at the *member scale*, rendering a robust material model for reinforced concrete. This robustness is a necessary prerequisite for the analysis of real-life structures such as reported in Part II of this paper: The RC cooling tower III Ptolemaïs SES (Greece) and the shotcrete tunnel shell installed at the Lainzer tunnel (Austria). Both structures were recently investigated at Vienna University of Technology.

Appendix

This appendix contains analytical solutions of the differential equation for the bond slip. The general form of this differential equation is given as

$$s''-cs^{\alpha}=0 \tag{37}$$

In the following, Eq. (37) will be solved for different cases arising from the employed bond stress–bond slip law.

Case 1: $\alpha=0$, $c>0$

The solution of the resulting linear differential equation $s''=c$ is obtained by integration

$$s=\frac{cx^2}{2}+C_1x+C_2 \tag{38}$$

where C_1 and C_2 = integration constants.

Case 2: $0<\alpha<1$, $c>0$

This nonlinear differential equation is solved by choosing s'' as (Vismann 1995)

$$s''=kx^p \tag{39}$$

Integration of Eq. (39) yields

$$s'=\frac{k}{p+1}x^{p+1}+C_1 \quad \text{and} \quad s=\frac{k}{(p+1)(p+2)}x^{p+2}+C_1x+C_2 \tag{40}$$

The nonlinear part of the bond slip–bond stress relation considered in this case is only relevant at the onset of bond slip, characterized by $s=0$ and $s'=0$. Accordingly, C_1 and C_2 in Eq. (40) become zero for a coordinate system with its origin placed at the mentioned onset point. Inserting s and s'' into the differential equation one gets

$$kx^p=c\left(\frac{k}{(p+1)(p+2)}x^{p+2}\right)^{\alpha} \tag{41}$$

A comparison of the power of x and of the coefficient yields

$$p=(p+2)\alpha \quad \text{and} \quad k=\frac{ck^{\alpha}}{(p+1)^{\alpha}(p+2)^{\alpha}} \tag{42}$$

finally giving

$$p=\frac{2\alpha}{1-\alpha} \quad \text{and} \quad k=\left(\frac{c}{(p+1)^{\alpha}(p+2)^{\alpha}}\right)^{1/1-\alpha} \tag{43}$$

Case 3: $\alpha=1$, $c<0$

For the differential equation of the type $s''-cs=0$ one obtains the characteristic equation using $s=e^{\lambda x}$, giving in $s''=\lambda^2e^{\lambda x}$, as

$$\lambda^2-c=0 \rightarrow \lambda=\pm\sqrt{c} \quad \text{where} \quad c<0 \tag{44}$$

The solution for this case is given by

$$\begin{aligned} s&=C_1e^{i\sqrt{-c}x}+C_2e^{-i\sqrt{-c}x} \quad \text{or} \\ s&=C_1^*\cos\sqrt{-c}x+C_2^*\sin\sqrt{-c}x \end{aligned} \tag{45}$$

with the constants C_1 and C_2 (or C_1^* and C_2^*).

Notation

The following notation is used in this paper:

A_c = concrete area of reinforced-concrete bar;
A_s = steel area of reinforced-concrete bar;
a_s = steel area per unit length;
c = concrete cover;
$d_{\max}$ = maximum aggregate size of concrete;
E_c = Young's modulus of concrete;
E_{c0} = reference value for Young's modulus of concrete;
E_s = Young's modulus of steel;
f_{cu} = uniaxial compressive strength of concrete;
f_{cu0} = reference value for uniaxial compressive strength of concrete;
$f_{cu,\text{cube}}$ = uniaxial compressive strength of concrete obtained from cubic specimens;
f_{sy} = yield stress of steel;
f_{tu} = uniaxial tensile strength of concrete;
G^f = fracture energy of concrete;
G_0^f = reference value for fracture energy of concrete;
h = height of concrete member for one layer of reinforcement;
$h_{c,\text{eff}}$ = effective tension height of concrete;
k = constant parameter;
ℓ = length of one-dimensional composite model at *bar scale;*
ℓ_c = width of plastic zone within fracture energy concept related to size of finite element;
ℓ_s = average crack spacing in reinforced concrete;
$\ell_{s,\max}$ = maximum crack spacing in reinforced concrete;
ℓ_s^{red} = *artificially reduced* average crack spacing in reinforced concrete;
$\ell_{s,p}^{\text{red}}$ = *artificially reduced* average spacing of cracks normal to reinforcement in p direction;
$\ell_{s,q}^{\text{red}}$ = *artificially reduced* average spacing of cracks normal to reinforcement in q direction;
n = ratio between Young's moduli of steel and concrete;
n_s = number of steel bars per unit length;
p_{bs} = force transferred by means of bond stress;
p_c = force acting on concrete bar;
p_s = force acting on reinforcement bars;
p_{sc} = force acting on uniaxial composite structure;
$\overline{q}$ = tensile strength of steel/concrete;
s = bond slip;
s_1, s_2, s_3 = material parameters describing bond stress–bond slip relation;
t = height of concrete member for two layers of reinforcement;
$\mathbf{u}$ = displacement vector;
u = displacement for uniaxial loading;
u_c = displacement of concrete at the crack face;
u_s = displacement of steel at the crack face;
$[\![u]\!]$ = crack width;
$[\![\overline{u}]\!]$ = calibration parameter for fracture criterion;
$\mathcal{W}$ = energy released in consequence of cracking of concrete and bond slip;
$\mathcal{W}_s$ = strain energy of bare steel bars;
$\mathcal{W}_{sc}$ = strain energy of composite material;
x = height of compression zone in concrete member; and local coordinate for analytical solution of bond slip;
$\overline{x}$ = position of crack face given in the local coordinate of analytical solution of bond slip;
x_n = coordinate normal to crack;
α = internal variable of fracture criterion;
$\overline{\alpha}$ = calibration parameter of fracture criterion;
β = dimensionless parameter for consideration of tension stiffening;
$\boldsymbol{\varepsilon}^p$ = tensor of plastic strains;
ε^p = uniaxial plastic strain;
ε_c = uniaxial strain in concrete;
ε_s = uniaxial strain in steel;

θ_p = angle between direction of reinforcement (p) and the normal to the crack;
π = 3.14...;
ρ_s = reinforcement ratio, given by $a_s/h_{c,\mathrm{eff}}$;
σ = uniaxial stress;
σ_c = uniaxial stress in concrete;
σ_s = uniaxial stress in steel;
τ = bond stress;
τ_f, $\tau_{\max}$ = material parameters describing bond stress–bond slip relation; and
$\varnothing_s$ = diameter of reinforcement bar.

References

Ben Romdhane, M., Rossi, R., and Ulm, F.-J. (1998). ''Micro-mechanical analysis of the steel-concrete interface behaviour.'' *Computational Modelling of Concrete Structures, Proceedings of the EURO-C 1998 Conf.*, R. de Borst, N. Bićanić, H. Mang, and G. Meschke, eds., Badgastein, Austria, Balkema, Rotterdam, The Netherlands, 731–740.

Comité Euro-International du Béton-Fédération International de la Précontrainte (CEB-FIP). (1990). *Model code 1990, bulletin d'information*. CEB, Lausanne, Switzerland.

Choi, C.-K., and Cheung, S.-H. (1996). ''Tension stiffening model for planar reinforced concrete members.'' *Comput. Struct.*, 59(1), 179–190.

Ciampi, V., Eligehausen, R., Bertero, V., and Popov, E. (1981). ''Analytical model for deformed bar bond under generalized excitations.'' *IABSE Colloquium on Advanced Mechanics of Reinforced Concrete*, Delft, The Netherlands, 53–74.

Ciampi, V., Eligehausen, R., Bertero, V., and Popov, E. (1982). ''Analytical model for concrete anchorages of reinforcing bars under generalized excitations.'' *Technical Rep. UCB/EERC-82/23*, Univ. of California, Berkeley, Calif.

Cox, J., and Herrmann, L. (1998). ''Development of a plasticity bond model for steel reinforcement.'' *Mech. Cohesive-Frict. Mater.*, 3, 155–180.

Dilger, W. (1966). ''Veränderlichkeit der Biege- und Schubsteifigkeit bei Stahlbetontragwerken und ihr Einfluß auf Schnittkraftverteilung und Traglast bei statisch unbestimmter Lagerung.'' Deutscher Ausschuß für Stahlbeton, 179 (in German).

Eligehausen, R., Popov, E., and Bertero, V. (1983). ''Local bond stress-slip relationships of deformed bars under generalized excitations.'' *Technical Rep. UCB/EERC-83/23*, Univ. of California, Berkeley, Calif.

Etse, G., and Willam, K. (1994). ''Fracture energy formulation for inelastic behavior of plain concrete.'' *J. Eng. Mech.*, 120(9), 1983–2011.

Feenstra, P. (1993). ''Computational aspects of biaxial stress in reinforced concrete.'' PhD thesis, TU Delft, The Netherlands.

Feenstra, P., and De Borst, R. (1995). ''Constitutive model for reinforced concrete.'' *J. Eng. Mech.*, 121(5), 587–595.

Floegl, H., and Mang, H. (1982). ''Tension stiffening concept based on bond slip.'' *J. Struct. Eng.*, 108(12), 2681–2701.

Harajli, M., Hout, M., and Jalkh, W. (1995). ''Local bond stress-slip behavior of reinforcing bars embedded in plain and fiber concrete.'' *ACI Mater. J.*, 92(4), 343–354.

Hillerborg, A., Modeer, M., and Petersson, P. (1976). ''Analysis of crack formation and crack growth in concrete by means of fracture mechanics and finite elements.'' *Cem. Concr. Res.*, 6, 773–782.

Huemer, T., Lackner, R., and Mang, H. (1999). ''Implementation and application of an algorithm for incremental adaptive finite element analysis of concrete plates.'' *Mechanics of quasi-brittle materials and structures*, G. Pijaudier-Cabot, Z. Bittnar, and B. Gérard, eds., Hermes Science Publications, Prague, Czech Republic, 331–352.

Kollegger, J. (1988). ''Ein Materialmodell für die Berechnung von Stahlbetonflächentragwerken.'' PhD thesis, Gesamthochschule Kassel, Germany.

Kwak, H., and Filippou, F. (1995). ''A new reinforcing steel model with bond slip.'' *Struct. Eng. Mech.*, 3(4), 299–312.

Lackner, R., and Mang, H. A. (2003). ''Scale transition in steel-concrete interaction. II: Applications.'' *J. Eng. Mech.*, 129(4), 403–413.

Martin, H., and Noakowski, P. (1981). ''Verbundverhalten von Beton-Stählen: Untersuchung auf der Grundlage von Ausziehversuchen.'' *Deutscher Ausschuß für Stahlbeton*, 319, 100–175 (in German).

Meschke, G., Lackner, R., and Mang, H. (1998). ''An anisotropic elastoplastic-damage model for plain concrete.'' *Int. J. Numer. Methods Eng.*, 42(4), 703–727.

Monti, G., and Spacone, E. (2000). ''Reinforced concrete fiber beam element with bond-slip.'' *J. Struct. Eng.*, 126(6), 654–661.

Ngo, D., and Scordelis, A. (1967). ''Finite element analysis of reinforced concrete beams.'' *J. Am. Concr. Inst.*, 64, 152–163.

Oliver, J. (1989). ''A consistent characteristic length for smeared cracking models.'' *Int. J. Numer. Methods Eng.*, 28, 461–474.

Pivonka, P., Lackner, R., and Mang, H. (2001). ''Material modelling of concrete subjected to multiaxial loading: Application to pull-out analyses.'' *Arch. Mech.*, 53(4–5), 487–499.

Rehm, G. (1961). ''Über die Grundlagen des Verbundes zwischen Stahl und Beton.'' *Deutscher Ausschuß für Stahlbeton*, 138 (in German).

Rostásy, F., Koch, R., and Leonhardt, F. (1976). ''Zur Mindestbewehrung für Zwang von Außenwänden aus Stahlleichtbeton.'' Deutscher Ausschuß für Stahlbeton, 267 (in German).

Vismann, U. (1995). ''Zuverlässigkeitstheoretische Verifikation von Bemessungskriterien im Stahlbetonbau.'' PhD thesis, Munich Univ. of Technology, Germany (in German).